

Spectral analysis of induced color change on periodically nanopatterned silk films

Jason J. Amsden¹, Hannah Perry¹, Svetlana V. Boriskina², Ashwin Gopinath², David L. Kaplan¹, Luca Dal Negro², and Fiorenzo G. Omenetto^{1,3,*}

¹Department of Biomedical Engineering, Tufts University, 4 Colby St Medford MA 02155 USA

²Department of Electrical and Computer Engineering & Photonics Center, Boston University, 8 Saint Mary's St., Boston, MA, 02215 USA

³Department of Physics, Tufts University, 4 Colby St Medford MA 02155 USA

*fiorenzo.omenetto@tufts.edu

Abstract: We demonstrate controllable structural color based on periodic nanopatterned 2D lattices in pure protein films of silk fibroin. We show here periodic lattices in silk fibroin films with feature sizes of hundreds of nanometers that exhibit different colors as a function of varying lattice spacing. Further, when varying the index of refraction contrast between the nanopatterned lattice and its surrounding environment by applying liquids on top of the lattices, colorimetric shifts are observed. The effect is characterized experimentally and theoretically and a simple example of glucose concentration sensing is presented. This is the first example of a functional sensor based on silk fibroin optics.

©2009 Optical Society of America

OCIS codes: (220.4000) Microstructure fabrication; (220.4241) Nanostructure fabrication; (160.5470) Polymers; (160.1435) Biomaterials.

References and links

1. H. J. Jin, S. V. Fridrikh, G. C. Rutledge, and D. L. Kaplan, "Electrospinning Bombyx mori silk with poly(ethylene oxide)," *Biomacromolecules* **3**(6), 1233–1239 (2002).
2. H.-J. Jin, J. Park, V. Karageorgiou, U. J. Kim, R. Valluzzi, P. Cebe, and D. L. Kaplan, "Water-Stable Silk Films with Reduced β -Sheet Content," *Adv. Funct. Mater.* **15**(8), 1241–1247 (2005).
3. U. J. Kim, J. Park, C. Li, H. J. Jin, R. Valluzzi, and D. L. Kaplan, "Structure and properties of silk hydrogels," *Biomacromolecules* **5**(3), 786–792 (2004).
4. X. Wang, H. J. Kim, P. Xu, A. Matsumoto, and D. L. Kaplan, "Biomaterial coatings by stepwise deposition of silk fibroin," *Langmuir* **21**(24), 11335–11341 (2005).
5. G. H. Altman, F. Diaz, C. Jakuba, T. Calabro, R. L. Horan, J. Chen, H. Lu, J. Richmond, and D. L. Kaplan, "Silk-based biomaterials," *Biomaterials* **24**(3), 401–416 (2003).
6. C. Jiang, X. Wang, R. Gunawidjaja, Y. H. Lin, M. K. Gupta, D. L. Kaplan, R. R. Naik, and V. V. Tsukruk, "Mechanical Properties of Robust Ultrathin Silk Fibroin Films," *Adv. Funct. Mater.* **17**(13), 2229–2237 (2007).
7. T. Xu, N. Zhang, H. L. Nichols, D. Shi, and X. Wen, "Modification of nanostructured materials for biomedical applications," *Mater. Sci. Eng. C* **27**(3), 579–594 (2007).
8. Q. Lv, C. Cao, Y. Zhang, X. Ma, and H. Zhu, "Preparation of insoluble fibroin films without methanol treatment," *J. Appl. Polym. Sci.* **96**(6), 2168–2173 (2005).
9. J. A. Hagen, W. X. Li, H. Spaeth, J. G. Grote, and A. J. Steckl, "Molecular beam deposition of DNA nanometer films," *Nano Lett.* **7**(1), 133–137 (2007).
10. B. D. Lawrence, M. Cronin-Golomb, I. Georgakoudi, D. L. Kaplan, and F. G. Omenetto, "Bioactive silk protein biomaterial systems for optical devices," *Biomacromolecules* **9**(4), 1214–1220 (2008).
11. A. J. Steckl, "DNA - a new material for photonics?" *Nat. Photonics* **1**(1), 3–5 (2007).
12. Z. Yu, W. Li, J. A. Hagen, Y. Zhou, D. Klotzkin, J. G. Grote, and A. J. Steckl, "Photoluminescence and lasing from deoxyribonucleic acid (DNA) thin films doped with sulforhodamine," *Appl. Opt.* **46**(9), 1507–1513 (2007).
13. M. K. Gupta, S. K. Khokhar, D. M. Phillips, L. A. Sowards, L. F. Drummy, M. P. Kadakia, and R. R. Naik, "Patterned silk films cast from ionic liquid solubilized fibroin as scaffolds for cell growth," *Langmuir* **23**(3), 1315–1319 (2007).
14. F. G. Omenetto, and D. L. Kaplan, "A new route for silk," *Nat. Photonics* **2**(11), 641–643 (2008).
15. H. Perry, A. Gopinath, D. L. Kaplan, L. D. Negro, and F. G. Omenetto, "Nano- and Micropatterning of Optically Transparent, Mechanically Robust, Biocompatible Silk Fibroin Films," *Adv. Mater.* **20**(16), 3070–3072 (2008).
16. S. Sofia, M. B. McCarthy, G. Gronowicz, and D. L. Kaplan, "Functionalized silk-based biomaterials for bone formation," *J. Biomed. Mater. Res.* **54**(1), 139–148 (2001).
17. R. Dallapiccola, A. Gopinath, F. Stellacci, and L. Dal Negro, "Quasi-periodic distribution of plasmon modes in two-dimensional Fibonacci arrays of metal nanoparticles," *Opt. Express* **16**(8), 5544–5555 (2008).

18. A. Gopinath, S. V. Boriskina, N.-N. Feng, B. M. Reinhard, and L. Dal Negro, "Photonic-plasmonic scattering resonances in deterministic aperiodic structures," *Nano Lett.* **8**(8), 2423–2431 (2008).
19. E. G. Loewen, and E. Popov, *Diffraction Gratings and Applications* (M. Dekker, New York, 1997).
20. D. W. Mackowski, "Calculation of total cross sections of multiple-sphere clusters," *J. Opt. Soc. Am. A* **11**(11), 2851–2861 (1994).
21. A. Gopinath, S. V. Boriskina, B. M. Reinhard, and L. Dal Negro, "Deterministic aperiodic arrays of metal nanoparticles for surface-enhanced Raman scattering (SERS)," *Opt. Express* **17**(5), 3741–3753 (2009).
22. C. A. Browne, *A Handbook of Sugar Analysis* (John Wiley & Sons, New York, 1912).
23. C.-S. Cheng, Y.-Q. Chen, and C.-J. Lu, "Organic vapour sensing using localized surface plasmon resonance spectrum of metallic nanoparticles self assemble monolayer," *Talanta* **73**(2), 358–365 (2007).
24. M. D. Malinsky, K. L. Kelly, G. C. Schatz, and R. P. Van Duyne, "Chain Length Dependence and Sensing Capabilities of the Localized Surface Plasmon Resonance of Silver Nanoparticles Chemically Modified with Alkanethiol Self-Assembled Monolayers," *J. Am. Chem. Soc.* **123**(7), 1471–1482 (2001).
25. S. V. Boriskina, and L. Dal Negro, "Sensitive label-free biosensing using critical modes in aperiodic photonic structures," *Opt. Express* **16**(17), 12511–12522 (2008).
26. B. Cunningham, J. Qiu, P. Li, and B. Lin, "Enhancing the surface sensitivity of colorimetric resonant optical biosensors," *Sens. Actuators B Chem.* **87**(2), 365–370 (2002).
27. S. Lu, X. Wang, Q. Lu, X. Hu, N. Uppal, F. G. Omenetto, and D. L. Kaplan, "Stabilization of enzymes in silk films," *Biomacromolecules* **10**(5), 1032–1042 (2009).

1. Introduction

Over five millennia of history have accompanied the evolution of silk from a prized textile to a scientifically attractive fiber. The protein has recently found uses well beyond textile and medical suture applications that have been the main modes of utilization in the past. For example, the generation of hydrogels, ultrathin films, thick films, conformal coatings, 3D porous matrices, solid blocks, and fibers with diameters ranging from the nanoscale to several centimeters have been explored with implications in biomaterials and regenerative medicine [1–4]. The toughness of this natural fiber, unmatched in nature, confers impressive mechanical properties to silk-based materials which rival if not exceed its organic counterparts (such as Kevlar for instance [5]).

Purified silk fibroin aqueous solution extracted from silkworm silk can be formed into robust, free-standing films of controllable thickness ranging between tens of nanometers to hundreds of micrometers [2,4,6]. These films are formed by simple casting or spin-coating of purified silk solution which crystallizes upon exposure to air [2]. The films can be further stabilized by annealing with methanol to make them insoluble in water [2,7,8]. The resulting hardened pure silk film possesses surface quality and transparency which are ideally suited for use as optical substrate [9–12].

Previous investigations [1,4,13] on the material properties of silk have shown the potential of this biopolymer to be reshaped on the micro and nanoscale with resolution limits well below a few tens of nanometers. This affords the possibility of molding silk on scales commensurate with visible wavelengths, which, in combination with the favorable bulk optical properties of silk films, can offer a platform for the realization of micro and nanopatterned silk optical elements. This was explored adopting an analogous approach to soft transfer molding by pouring the purified silk solution on appropriate molds [10,14,15]. In this paper, we leverage the facile manufacturing processes of this material to generate periodic nanopatterned lattices on silk fibroin films and controllably generate spectral signatures as a function of the lattice spacing used on the film surface. Spectral characterization of the nanopatterned silk films is performed and the spectral responses of the geometries are theoretically calculated using both diffraction theory and generalized Mie scattering. Finally we show a simple proof of principle colorimetric sensor based on the fabricated nanophotonic crystal lattices for detection of glucose concentrations. This is the first example of a functional sensor based on silk fibroin optics.

2. Fabrication and properties: silk optical films

Forming optical structures and films from silk fibroin solution employs simple processing in an all-water environment at room temperature. Production of the silk fibroin solution has been previously described the literature [15,16]. Briefly, the purification of silk fibroin from

Bombyx mori cocoons initially involves the removal of sericin, a water-soluble glycoprotein which binds fibroin filaments, by boiling the cocoons in a 0.02 M aqueous solution of sodium carbonate for 60 minutes. After drying, the fibroin bundle is then dissolved in a 9.3 M aqueous solution of lithium bromide at 60°C for four hours. The lithium bromide salt is then extracted through a water-based dialysis process. The resulting solution is then centrifuged and filtered via syringe based micro-filtration (5 μm pore size, Millipore Inc., Bedford, MA) to remove any remaining particulates. This process enables the production of 8-10% w/v silk fibroin solution with minimal contaminants and reduced scattering for optical applications.

The masks used for fabrication of the silk nanostructures are created via optimized schemes for nanoscale electron-beam writing of hard metal masks. In particular, a high throughput process is used which guarantees 20 nm minimum feature size with complete reproducibility over 1 cm^2 chip areas using Cr metal on Si wafers [17,18]. For the results presented here, all the nanoparticles have a diameter of 200 nm and their separation varies according to a desired lattice constant A , representing the center to center separation of adjacent particles. The particles are 30 nm high. The silk solution is poured onto the masters and allowed to dry as previously described [15]. The resulting films are approximately 10 μm thick. The silk nanopatterned photonic lattices obtained through this fabrication method are then annealed with methanol and spectrally characterized. Figure 1(a) and (b) show SEM images of one of nanopatterned silk lattices with a lattice constant of 300 nm.

Upon illumination with broad spectrum visible light, the nanopatterned silk structures scatter light. Figure 1(c) shows a 4 x, 0.13 numerical (NA) microscope image of the nanopatterned silk structures illuminated with the dark field condenser. The resulting colour of the structures depends on the lattice spacing, angle of illumination and angle of collection. The lattice constant A (i.e. the center to center spacing between the holes) in the coloured squares from left to right in the figure are 700 nm, 600 nm, 500 nm, and 450 nm. Spectral characterization is accomplished by using dark-field illumination and imaging with a hyperspectral CCD (CRI Nuance FX) camera attached to an Olympus IX71 microscope. The objective used was an Olympus 4x, 0.13 NA UPlanFLN objective. The illumination was obtained by a dark-field condenser with NA 0.8-0.92 or nonlinear conversion of 100 fs 80 MHz laser pulses from a Spectra Physics Tsunami Ti:Sapphire oscillator in a high- Δ photonic crystal fiber. The generated supercontinuum was transferred through a multimode optical fiber (GIF625, Thorlabs, Inc.) which was fed through a micropipette tip on an Eppendorf NK2 micromanipulator. Using the micromanipulator, the fiber is positioned 100 μm from the surface of the patterned silk and positioned at an angle of 80° from the surface normal. At this distance, the divergence of the illuminating beam is small, so it can be considered a plane wave. Spectra are taken at 2 nm resolution using the Nuance camera and are normalized to the largest intensity without further processing.

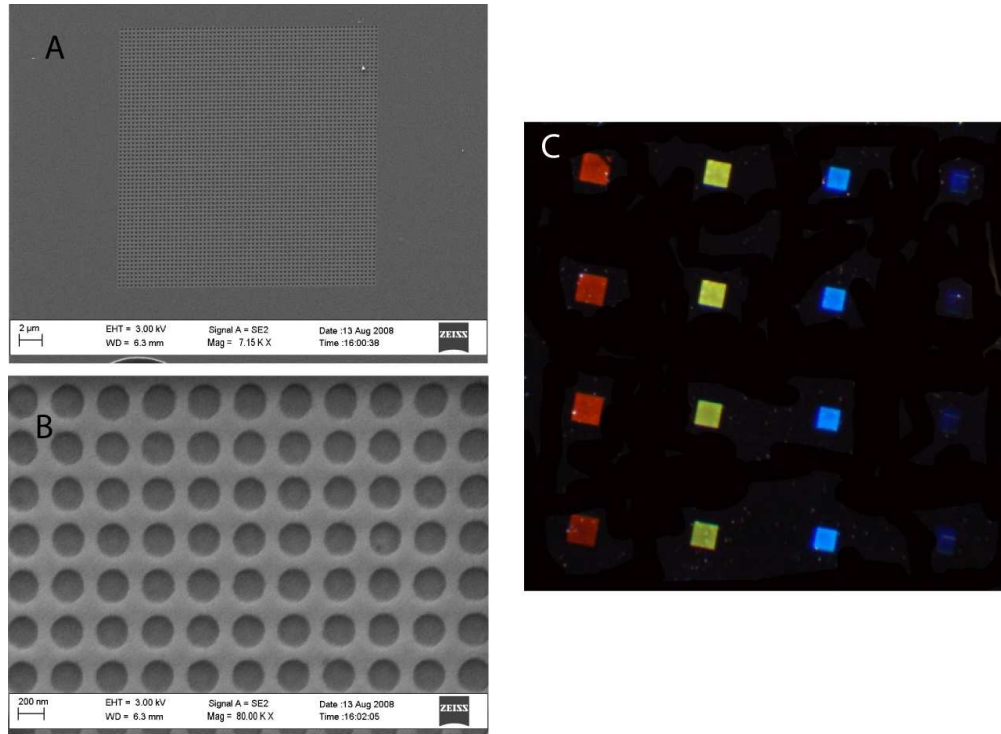


Fig. 1. A. SEM image of periodic nanoholes in silk. The nanoholes are 200 nm in diameter, 30 nm deep and separated by 300 nm. B) Magnified image of A. C) Periodic nanoholes in silk illuminated with light from a dark-field condenser. The lattice constants are from left to right 700, 600, 500, and 400 nm. The distance between the rows of colored squares is 200 μm .

Figure 2 shows the nanopatterned lattices illuminated with supercontinuum from an optical fiber placed 100 μm from the silk surface. Figure 2(a) shows the experimental geometry, while Fig. 2(b) shows the scattering from the nanopatterned silk. Upon immersion of the imprinted structures and the illuminating fiber in water, there is a red shift in the scattered colours collected by the microscope objective due to the change in index between water ($n_{\text{water}} = 1.333$) and air ($n_{\text{air}} = 1.000$). This is shown in Fig. 2(b).

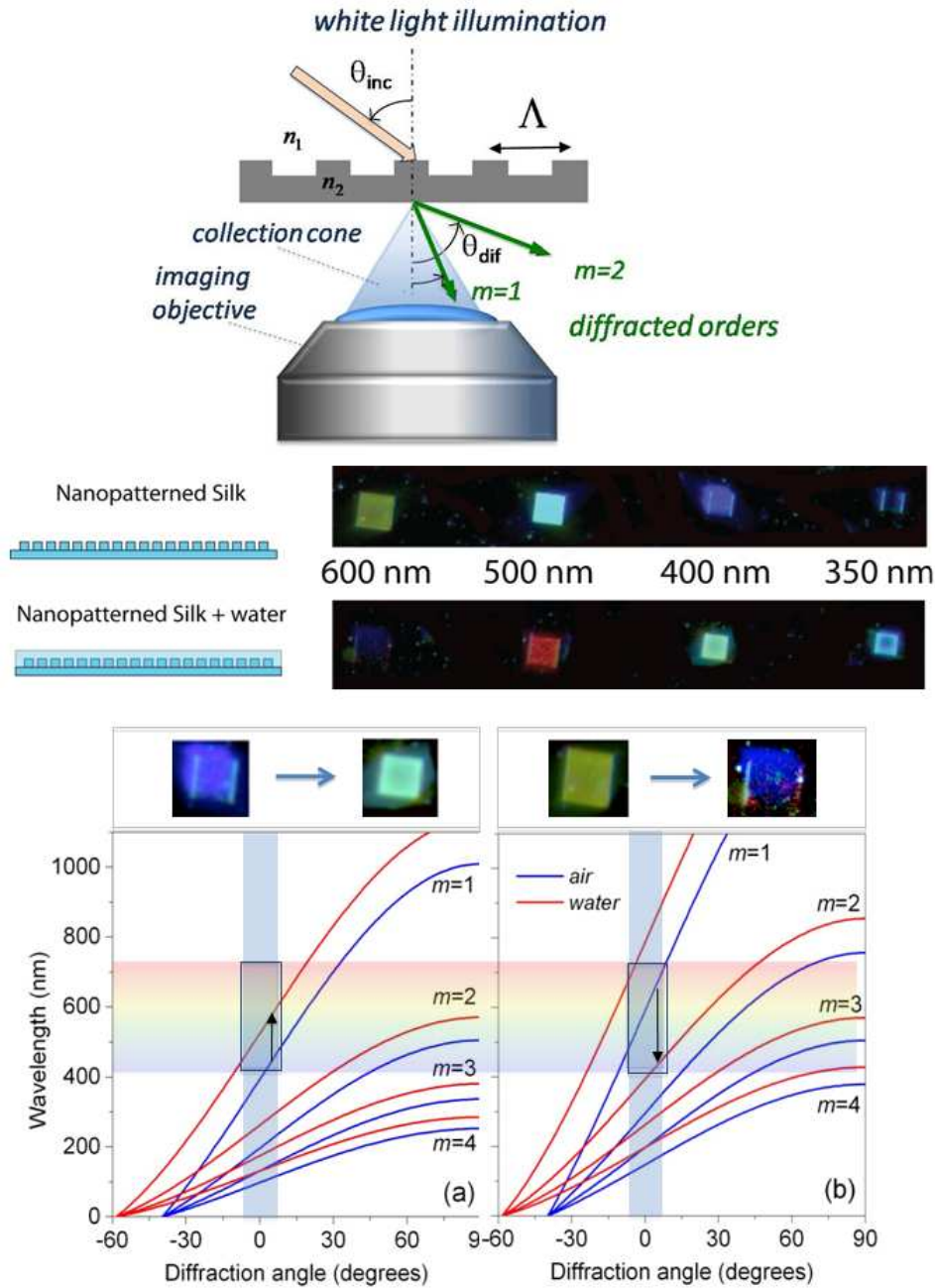


Fig. 2. (a) Experiment geometry. (b) Periodic imprinted nanoholes 200 nm in diameter and 30 nm deep illuminated with supercontinuum. The lattice constants Λ vary from right to left in the figure: 600 nm, 500 nm, 400 nm and 350 nm. The spacing between the colored squares is 200 μm . In the upper panel, the medium above the holes is air. In the bottom panel the medium above the holes is water. (c) Wavelength versus the diffracted angle for the first four diffractive orders of the silk gratings with the periods of 400 nm (i) and 600 nm (ii) ($n_2 = 1.54$, $\theta_{inc} = 80^\circ$). The shaded areas cover the parameter range observable in the experiment (within the visible spectrum frequency band and within the collection cone). The direction of the incident beam is exaggerated for clarity.

The mechanism of structural colour and structural colour shift upon immersion of the structures in different index fluids can be qualitatively understood with classical diffraction theory of periodic gratings. The specific scattering angles for a given incident angle are described in Eq. (1) [19].

$$\lambda = \frac{\Lambda}{m} (n_1 \sin \theta_{inc} + n_2 \sin \theta_{dif}), \quad m = 0, \pm 1, \pm 2 \quad (1)$$

Λ is the lattice (grating) constant, λ is the wavelength of the incident light, θ_{inc} and θ_{dif} are the incident and diffracted angles (measured with respect to the normal to the grating surface), m is the diffraction order and n_1 and n_2 are the refractive indices the surrounding media and of the silk, respectively. Figure 2(a) shows a schematic of the grating and the angle definitions. Because light is collected by the objective within a cone defined by the objective numerical aperture (in our experiments, $NA = 0.13$, $-7.5^\circ \leq \theta_{dif} \leq 7.5^\circ$), only a portion of an order is collected. A change in the refractive index of the surrounding medium shifts the diffraction angles of all the grating orders determining the structural colour response of the silk nanostructures. This effect is shown in Fig. 2(c), which shows calculated scattered wavelengths corresponding to the first four diffraction orders, the diffraction angles, and the collection angle limitation imposed by the objective. Depending on the grating period and the refractive index change, two situations are possible: the same grating order m is collected and a red-shift in wavelength is observed, or the successive grating order $m + 1$, is collected, resulting in a blue-shift of the structural colour

Additionally, in order to demonstrate the effect of angular redistribution of light scattered by 2D periodic gratings with the ambient refractive index change, we have calculated the field scattered by a periodic array of silk spheres (200 nm diameter and 500 nm lattice constant) embedded either in air or in water, as shown in Figs. 3(a)-3(d). The periodic array was illuminated by plane waves of three different wavelengths (falling within the blue, green and red parts of the visible spectrum) at almost grazing incidence ($\theta_{inc} = 80^\circ$). The incident field was subtracted from the spatial field distribution in order to better approximate the conditions of the dark-field scattering experiments. The scattered fields are calculated using the Generalized Mie Theory (GMT), which is a rigorous solution of the full-vector Maxwell's equations [18,20]. Although GMT is limited to the simulations of the spherical shapes, it provides a very powerful and efficient tool for studying the effects of arrays morphologies on their scattering characteristics and can be used to approximate scattered fields in 2D gratings of arbitrarily-shaped particles [18,21]. The results of the GMT simulations are shown in Figs. 3(a)-3(d). Figures 3(a) and 3(b) show a side view of the grating (located in the x-y plane at $z = 0$); and the plane waves are incident from the bottom left at the angle of 80 degrees from the surface normal. It can be clearly seen that although most of the incident light is forward-scattered, the periodic grating redistributes the illumination intensity into markedly different directions depending on the refractive index of the embedding medium. A limited collection cone (defined by the numerical aperture of the microscope objective) provides angular filtering of collected light resulting in the colour response observed in the experiments. This effect is demonstrated in Figs. 3(c) and (d), present the scattered field patterns at three wavelengths in the plane parallel to the grating located at the arbitrarily chosen distance of 100 micron above the grating plane to illustrate the shift in observed colour.

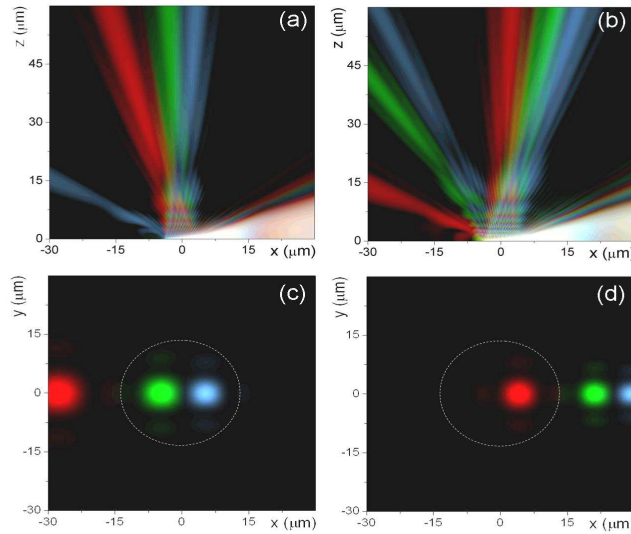


Fig. 3. Electric field scattered by a periodic grating of 256 200 nm diameter silk spheres with a lattice constant of 500 nm in air (a,c) and water (b,d). Plane waves of $\lambda = 470$ nm (blue), $\lambda = 520$ nm (green), and $\lambda = 630$ nm (red) are incident at 10 degrees angle to the array plane and scatter into well-defined grating orders (a,b). (c,d) The scattered electric field distributions in the plane 100 μm above the grating (top view). The circles represent a cross-section of the collection cone of a microscope with $\text{NA} = 0.13$ (± 7.5 degrees)

3. Colorimetric sensing

The mechanism of color change presented above can be used as a basis for sensing in which the difference between the index of refraction of the nanostructure and its surroundings determine a spectral shift that can be used as a transduction variable. To this end, we use the nanopatterned periodic arrays described above to characterize different concentrations of glucose by depositing a sample onto the lattice and characterizing its spectral response

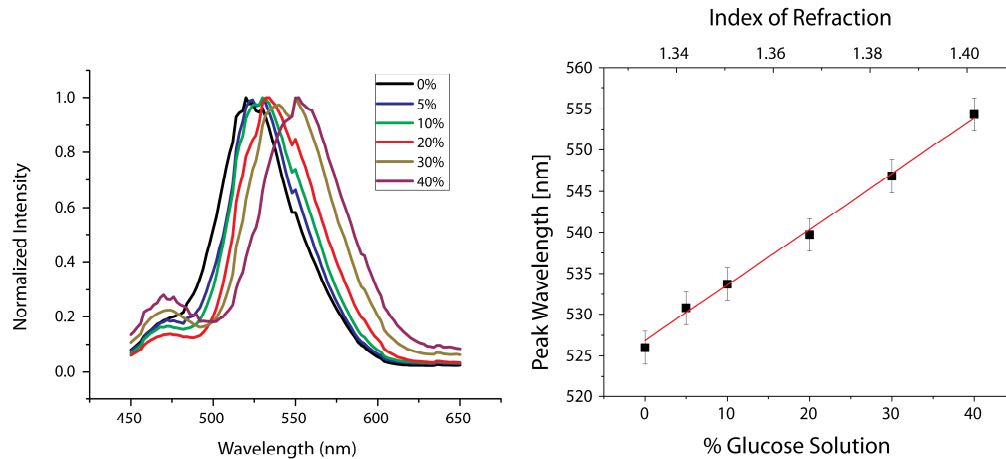


Fig. 4. Experimental structural color change with varying refractive index. (a) Spectra of the 400 nm lattice constant structure illuminated with supercontinuum with different concentrations of glucose. (b) Plot of the peak in (a) vs. glucose concentration and index of refraction.

We used several different aqueous solutions of glucose (0, 5, 10, 20, 30, and 40% by weight) which have well known refractive index [22]. Figure 4(a) displays the scattering spectra obtained using the structure with lattice constant $\Lambda = 400$ nm for the different concentrations of glucose and Fig. 4(b) shows a plot of the peak scattered wavelength vs. the glucose concentration and refractive index. The peak at 526 nm for 0% glucose progressively red-shifts with increasing glucose concentration and index of refraction. The results illustrate that the device is sensitive to a change in index $\Delta n = 0.007$ which corresponds to a change in glucose concentration of 5%.

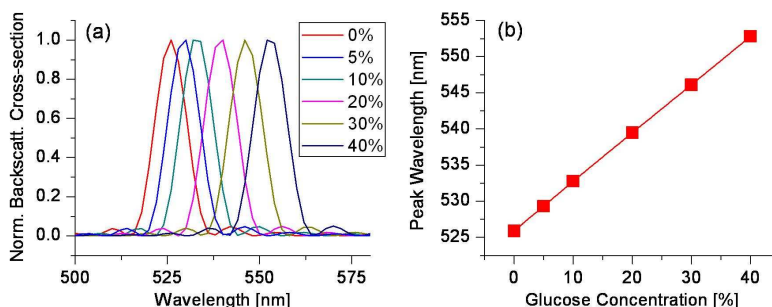


Fig. 5. Theoretical calculation for refractometric sensing with periodic silk gratings: (a) Normalized back-scattering cross-section of a grating composed of 256 100nm-radius silk spheres with a lattice constant of 600 nm immersed in water and glucose solutions and illuminated by a plane wave at 10 degrees to the array plane; (b) Shift of the peak wavelength as a function of the glucose concentration in the solution.

In excellent agreement with experimental data shown in Fig. 4, the calculated frequency spectrum of the back-scattering cross section of a periodic array of 200 nm diameter silk spheres with 400 nm lattice constant shown in Fig. 5(a) features a pronounced peak at 526 nm. This peak progressively red-shifts with the change of the ambient refractive index from that of water to 40% glucose solution. The calculated peak wavelength as a function of the glucose concentration is shown in Fig. 5(b).

The refractive index sensitivity (defined as the ratio of the wavelength shift caused by the change of the ambient refractive index to the value of the index change) is estimated as 400 nm/RIU (RIU = refractive index unit). This value exceeds experimentally reported typical sensitivity values of surface-plasmon biosensors based on periodic arrays of noble metal particles (ranging from 150 to 250 nm/RIU for $\lambda \sim 600$ nm operating wavelength [23,24]) and those of dielectric-grating-based biosensors exploiting the mechanism of resonant reflection (88-271 nm/RIU for $\lambda \sim 850$ nm [25]). Further experiments with different nanopatterned lattices including the use of aperiodic patterns [26] could lead to increased sensitivity and are the subject of future study.

4. Conclusion

In this paper, we demonstrate controllable structural color based on periodic nanopatterned 2D lattices in pure protein films of silk fibroin. We show here periodic lattices in silk fibroin films with feature sizes of hundreds of nanometers that exhibit different colors as a function of varying lattice spacing. Further, when varying the index of refraction contrast between the nanopatterned lattice and its surrounding environment by applying a liquid on top of the lattices, colorimetric shifts are observed. The effect is characterized experimentally and theoretically and a simple example of glucose concentration sensing is presented.

The work presented here represents a set of baseline measurements for future work that will leverage a distinguishing feature that sets optical elements realized in silk apart from conventional optical materials. Silk devices are biocompatible and have been demonstrated to entrain and maintain biological activity within the silk optical elements by simple mixing of biological dopants in the silk fibroin solution used as a precursor to form optical elements.

Because of the gentle processing environment and the properties of the material, these “natural” dopants such as proteins, organic molecules, enzymes or antibodies maintain function within the hardened silk matrix, and can be handled and stored for extended time frames under ordinary laboratory conditions without the need for refrigeration or controlled temperatures [10,27]. Other advantages of the demonstrated low-index biosensor platform include cost-efficient, large-scale device replication, potential for the integration with microfluidics, and compatibility with microarray-based infrastructures that are widely used for high throughput bimolecular interaction analyses. This will enable a new class of “biologically active optics” that would not be otherwise obtainable in more commonly used materials such as organic polymers, glasses or semiconductors, which require processing conditions (such as high temperature, acid or base processing or high pressures, for instance) that do not support the retention of function of labile biological components.

Acknowledgements

The authors thank Prof. Daniel Mackowski for useful discussions and for making his Fortran codes available for public use. This material is based upon work supported in part by the U.S. Army Research Laboratory and the U.S. Army Research Office under contract number W911 NF-07-1-0618 and by the DARPA-DSO.